Design of a Concrete-Based Sensible Heat Storage Module Prototype for Solar Heat

Federico H. Licandro[1], Pedro A. Galione[1], Joaquin Buydid[2] and Emmanuel Romano[2]

[1] Facultad de Ingeniería, Universidad De La República (Montevideo, Uruguay)

[2] VÖLFER Ingeniería (Paso de los Toros, Uruguay)

Abstract

One of the main challenges associated with solar power is its dependence on sunlight. Previous research has shown that storage systems can help match energy production with its demand. The present work focuses on the design, construction, and evaluation of a concrete-based sensible heat storage module for a solar process heat plant. A combination of experimental, analytical and numerical methods is implemented to evaluate the heat transfer, pressure drop, and capital cost of different design options. After selecting geometry and concrete recipe, a storage module is constructed and operated in a prototype facility for producing hot fluid at 150°C. This is part of a collaborative effort between academic and industrial partners to develop scalable, cost-effective solar thermal solutions for industrial processes.

Keywords: Sensible Heat Thermal Energy Storage, Solar heat for industrial process, Concrete, numerical heat transfer, industry-academia collaboration.

1. Introduction

The rising energy demand, coupled with global efforts to reduce fossil fuel consumption, has accelerated the adoption of renewable energy sources in recent years, such as solar heat for industrial processes (SHIP). One of the most important challenges posed by the implementation of alternative energy sources is their dependence on resource availability. Thermal Energy Storage (TES) systems help address this issue by storing excess energy when supply exceeds demand, making it available when supply drops or demand rises. TES not only enhances the reliability of solar thermal technologies but, when properly implemented, can also improve cost-effectiveness, efficiency, and environmental impact [Sarbu & Sebarchievici, 2018].

TES technologies are typically classified into three groups: sensible heat storage (SHTES), latent heat storage (e.g., phase change materials), and thermochemical storage (TCS). Concrete is an appealing material for SHTES due to its thermomechanical properties, low cost, and high availability [Laing & Lehmann, 2009; Dellicompagni et al., 2016].

In Uruguay, the solar industry remains underdeveloped despite possessing solar resources comparable to leading countries like Spain [Bosquera et al., 2021]. To support development and promote national technological progress, a SHIP prototype is proposed with low investment costs and the ability to store energy as sensible heat using a concrete-based module. This study, part of an industry-academia collaboration, focuses on the design and development of the energy storage system. It presents the design process of a concrete TES unit for a SHIP prototype plant, considering hydraulic, thermal, and economic aspects, with an emphasis on heat transfer modeling and low-cost solutions. The design of other installation components is explained in other papers presented at this congress.

The installation prototype consists of three main components (Figure 1): the solar collectors, the Concrete Storage Unit (CSU), and a heat exchanger (heat dump) which simulates heat delivery to an industrial process. The heat dump projected for the prototype installation is a low-pressure steam generating vessel

with a coil, inside which the heat transfer fluid (a mixture of water and glycol) flows. During the heat dump operation period (heat demand), the heat transfer fluid transports thermal energy from the solar collector or a previously heated concrete storage unit to the heat exchanger; during the non-operation period (heat surplus), solar heat can be used for CSU charging.

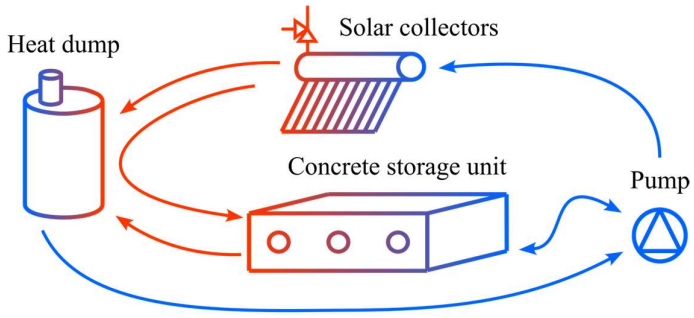

Figure 1: Prototype installation operation scheme.

2. Design considerations

De The design prototype CSU has a capacity of 30 kWh, consisting of 3 hours of storage at the plant's nominal power (10 kW). Since the solar collectors are of CPC type, a maximum temperature of 160ºC is specified. To enable storage of energy as sensible heat in the CSU, a temperature difference of around 25–30ºC is considered between the hot and cold branches of the prototype installation, which allows simulating industrial process vapor production at around 130ºC. The system control is designed to vary the flow rate to maintain the maximum temperature at the desired level, while the cold temperature is determined by the heat dump design and operation.

The CSU consists of an array of glycolated water-filled pipes embedded in a concrete matrix. As the pumping system has already been selected, the pressure drop at the maximum flow rate is limited. Therefore, CSU design is restricted to shape, dimensions, and geometry selection, as well as concrete mix design and additive formulation. The goal is to maximize thermal performance, minimize hydraulic losses, and reduce costs.

The optimal thermal behavior of the CSU should guarantee a constant maximum charging/discharging rate, as well as stable outlet temperatures. However, as concrete absorbs/releases energy, its temperature changes, gradually reducing the heat flux between the heat transfer fluid and the CSU, and eventually causing variations in outlet temperature during operation. Thermal stratification [Haller et al., 2009] of the CSU can help mitigate the loss of thermal potential during charging/discharging periods; if the CSU is perfectly stratified, energy is stored as a "horizontal piston," maintaining concrete regions at their original thermal potential. Conversely, if the storage unit is poorly stratified, temperature increases uniformly throughout the concrete volume, lowering the temperature inside the entire CSU and therefore reducing the heat flux (a sketch of this behavior is presented in Figure 2).

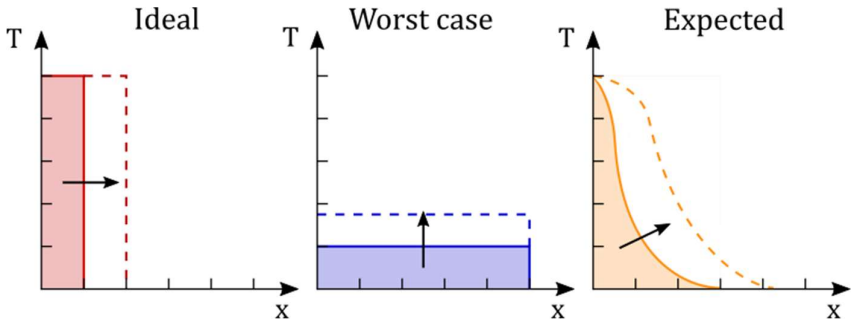

Figure 2: Different charging profiles for the CSU: perfectly stratified, poorly stratified, expected scenario. Coordinate *x* is aligned with the advance of the heat transfer fluid.

Even though perfect stratification of the CSU is impossible (due to the diffusive nature of thermal energy),

shape design and material selection should aim for a charging/discharging profile with high thermal stratification. Higher thermal stratification occurs when heat transfer in the fluid flow direction is smaller than in the transversal directions. Prioritization of the transversal heat flow can be achieved by reducing the thermal resistance in the transversal directions and increasing it in the principal flow direction; therefore, CSU length (parallel to flow direction) should be considerably greater than its other dimensions. If the CSU is large enough, thermal conduction in the axial direction within the concrete should be negligible when compared to fluid-wall convection and transversal heat conduction.

Reducing water advection could also enhance thermal stratification. Thermal energy conservation equation can be applied to a water region Ω; assuming that thermal diffusivity is negligible (in the axial direction) when compared to advective and convective terms, the energy conservation equation for the region Ω is as presented in Equation 1; Where m is the heat transfer fluid mass in the Ω region, C_p the heat capacity at constant pressure, T_m the volume averaged temperature, $\dot{m}$ the mass flow rate, T_2 and T_1 the temperatures at the region outlet and inlet respectively, h the convective heat transfer coefficient, A the heat transfer area and $\overline{T_S}$ the average surface temperature.

$$\frac{m}{\dot{m}}\frac{\partial}{\partial t}T_m + (T_2 - T_1) = -\frac{hA}{\dot{m}C_p}(T_m - \overline{T_S}) \quad \text{(eq. 1)}$$

Note that the transversal heat transfer relative value grows the higher the $NTU = hA/\dot{m}C_p$ coefficient. Higher inlet to outlet temperature difference $T_1 - T_2$ implies better thermal stratification. Inlet to outlet temperature difference can be increased by an increase of the *NTU* coefficient or an increase of the heat transfer potential $T_m - \overline{T_S}$.

Given that the heat transfer fluid flow rate is determined by the operating conditions of the prototype installation, the NTU coefficient can be increased by extending the pipe length, using pipes with larger diameters, and/or installing a greater number of pipes. If all other dimensions are fixed (diameter and number), increasing the pipe length results in a larger heat transfer area without altering the heat transfer coefficient, although it leads to a higher pressure drop. Alternatively, increasing the number or diameter of the pipes while keeping the length constant also enhances the heat transfer area while reducing pressure drop, however, the heat transfer coefficient decreases. If the Reynolds number drops below the critical threshold, the flow may become laminar, which can significantly reduce the NTU coefficient despite the increase in heat transfer area. All the aforementioned design alternatives lead to higher CSU construction costs.

Transversal heat transfer can also be improved by reducing the average surface temperature, which strongly depends on the thermal properties of the concrete, such as thermal conductivity and heat capacity. Higher thermal conductivity reduces conduction resistance, facilitating heat flow within the concrete region and thereby lowering the surface temperature. This, in turn, increases the thermal potential $T_m - \overline{T_S}$.

The required concrete mass M is directly proportional to its heat capacity C for a given SSHTES Thermal Energy Storage Capacity *TESC* and temperature potential (T_{max} and T_{min}) as expressed in Equation 2. The addition of concrete mass has the potential to increase either the transversal or axial thermal resistance, depending on whether the mass is added laterally or longitudinally. However, axial addition of concrete mass implies a greater pipe length, which in turn increases prototype fabrication costs. With cost-effectiveness mind, the addition of concrete mass increases transversal resistance. A higher concrete heat capacity potentially reduces transversal resistance, thereby improving thermal stratification; however, this alternative is not considered in the scope of the present study. Concrete mixture formulation for the prototype CSU aims for high thermal conductivity.

$$TESC = MC(T_{max} - T_{min}) \quad \text{(eq. 2)}$$

Heat losses through the CSU envelope should be minimized not only to improve system efficiency but also to extend the period during which stored thermal energy remains available. This, in turn, enhances the CSU's ability to mitigate the solar heat availability and industrial process energy demand mismatch.

3. Methodology

CSU design is separated into two main work lines: Concrete recipe formulation, testing and evaluation; and CSU geometry and dimension specification. Concrete mixture formulation is derived from literature review; evaluation of thermal properties is carried by experimental testing. Geometry and dimension determination comes from a combination of numerical and analytical methods for heat transfer, pressure drop and component cost estimation.

3.1. Concrete mixture formulation and evaluation

Concrete mixture is selected with the aim of maximizing thermal conductivity. According to the literature, the thermal conductivity of concrete is directly proportional to the conductivity of the mortar, the conductivity of the stone aggregates in the mix, the percentage of metallic fibers in the matrix (provided there is good adhesion at the interface), and the moisture content. It decreases with increasing temperature and porosity. In general, conductivity is governed by the mortar and, consequently, by the aggregates: siliceous aggregates conduct heat better than calcareous ones, and since sand contains a high fraction of quartz (silica), the mix benefits from a suitable proportion of fines. For this prototype, granite aggregates with high silica content were chosen to achieve the target conductivity [Cook et al., 1974; Kodur et al., 2003; Asadi et al., 2018].

Studies also show that, as long as the interface between fibers and concrete is of good quality, thermal conductivity increases linearly with fiber content. The fibers act as thermal bridges, so good adhesion is essential for effectiveness. Hooked fibers are particularly recommended because they significantly improve bonding to the matrix, and high compaction of the mix is necessary to reach the desired performance [Siming Liang et al., 2023; Kodur et al., 2003; Zhang et al., 2023].

Other factors such as temperature, porosity, and moisture must also be considered. As temperature rises, conductivity decreases; Kodur et al. (2003) proposed an empirical expression for thermal conductivity as a function of temperature, $k = 2.5 – 0.0034\ T$, which indicates an expected approximate reduction of 20 % for T ~ 150 ºC. Porosity reduces conductivity, and excessive fiber addition may negatively impact compaction. Therefore, achieving maximum compaction with a low water-to-cement ratio is critical, while higher moisture content tends to increase conductivity [Asadi et al., 2018; Zhang et al., 2023]. In general, if the plain concrete has low conductivity, the addition of fibers produces little improvement; the base mix must perform adequately, with the other variables acting as multipliers.

A set of cylindrical specimens (10 cm in radius and 20 cm in length) were fabricated to evaluate thermal conductivity following the ASTM D5334-14 standard procedure (needle probe method for determining the thermal conductivity of soil and soft rock using a transient heat technique). To allow needle insertion into the concrete, axial holes with a 6 mm diameter and 7 cm depth were incorporated through each end face of the cylinders during fabrication. The tests were conducted at room temperature using a TEMPOS RK-3 needle probe, suitable for measuring thermal conductivities in the range of 0.1–6.0 W/mK [Tempos, 2024]. The experimental setup and sample geometry are shown in Figure 3.

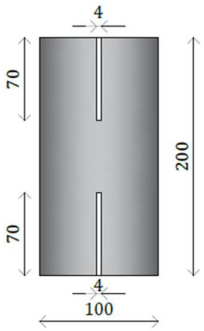

Figure 3: Photograph of a thermal conductivity measurement for a concrete sample and concrete sample geometry.

3.2. Heat transfer, hydraulic and cost analysis

Several design alternatives with the same heat transfer area are initially proposed. CSU heat transfer area is initially estimated with a simplified heat transfer model. Since the accumulator operates under transient conditions, the usual methods for recuperative heat exchangers, which are formulated for steady-state operation, cannot be directly applied. In this work, however, as an initial approach to estimate the required heat transfer surface area, an analysis based on recuperative exchanger formulations was carried out under several simplifying assumptions. The method assumes that, although both the solid (concrete) and the fluid undergo temporal temperature variations, their axial temperature profiles evolve while maintaining an approximately constant "mean" temperature difference throughout the process. Under this assumption, the expression given in Eq. 11 can be used to calculate the "mean" transferred power (Qst).

$$\dot{Q}_{st} = UA_{st}\Delta T_{mean} \quad \text{(eq. 3)}$$

where $(UA)_{st}$ is the product of the overall heat transfer coefficient and the heat transfer area, and ΔT_{mean} is the mean temperature difference between the fluid and the storage material. By assuming reasonable values for U, the total heat transfer area (directly related to the pipe wall surface) can be estimated.

The estimation of U is performed by calculating the convective heat transfer coefficient of the fluid inside the pipes, the heat transfer resistance of the pipes' walls, and by estimating the equivalent heat transfer resistance of the portion of concrete near the walls (modeled as radial heat conduction at steady state). This last resistance depends on the thermally affected region within the concrete, which is here assumed to vary in a range of some diameters of distance from the center of the pipes. This distance is limited by half the distance between pipes.

For the design of alternative configurations, "mean temperature" differences between 3 and 10 °C are assumed. For a design heat transfer rate of 10 kW, this results in a range of overall heat transfer coefficient area products (UA) between 1000 and 3300 W/K. By imposing a convective heat transfer coefficient of 2000 W/m^2·K (more or less typical for water flow inside pipes), a concrete thermal conductivity of 2 W/m·K and varying the thermally affected zone within the concrete to be between 2 and 4 pipe diameters, U values result in the range of 180 - 320 W/m^{2}K. From this analysis, ranges of values of heat transfer area (pipe wall area) between 3 to 6 m^2 —if ΔT_{mean} is 3 ºC— and between 10 to 19 m^2 —if ΔT_{mean} is 10 ºC— are obtained.

Based on the above, a tentative heat transfer area of 12 m² is considered reasonable for initiating the heat exchanger design. Different combinations (alternatives) of tube number and length are proposed, with the same total area, and the configurations for which an acceptable pressure drop is expected are evaluated in more detail. By varying the pipe diameter between ⅛" and ¾", the total tube length varies from approximately 150 to 350 m. The total tube length implies that pipes should bend inside the concrete matrix, in order to obtain acceptable CSU bulk dimensions.

Pressure drop Δp predictions inside the CSU are made with Handbook of Hydraulic Resistance [Idel′chik, 1996] correlations. Generic total pressure drop of the CSU is presented in equation 4; where Δp_d is the distributed pressure drop, Δp_l is the local pressure drop caused by bends in flow direction, f is the friction coefficient, L is the pipe length, d is the pipe diameter, ρ the heat transfer fluid density, v the heat transfer fluid mean velocity, θ the bend angle, R_0 the bend curvature and N the number of bends in each pipline.

$$\Delta p = \Delta p_d + \Delta p_l = \frac{fL}{d}\frac{\rho v^2}{2} + 0.175\lambda\frac{R_0\theta}{d}N \quad \text{(eq. 3)}$$

Cost estimation of the CSU design uses local pricing of materials (pipes and concrete) as well as manufacturing costs, such as pipe bending costs.

Design alternatives of the CSU heat transfer are evaluated using numerical heat transfer equations (finite volumes method) through an OpenFOAM software implementation [Weller et al., 1998] with a multi-region solver. The multi region solver calculates the velocity field for the fluid region, and the temperature field for every region. Charging and discharging stages are simulated for different geometries, thermal stratification of the CSU alternatives are evaluated by comparing energy storage and charging heat rates.

Computational costs are reduced by domain simplification. The fluid domain is discretized only along the axial direction, assuming cylindrical symmetry and negligible radial variation. Heat transfer at the fluid–wall interface is modeled using convective heat transfer correlations (equation 4) [Mikheyev, 1968], with

convection coefficients of approximately 2000 W/m²K imposed for the different configurations. The solid concrete domain is discretized in 3D. The geometry is simplified to an extruded tube, with the domain reduced through symmetry and adiabatic boundary conditions. A cross-section of the mesh perpendicular to the flow is shown in Figure 4, where symmetry planes and the different regions (water, pipe and concrete) are identified.

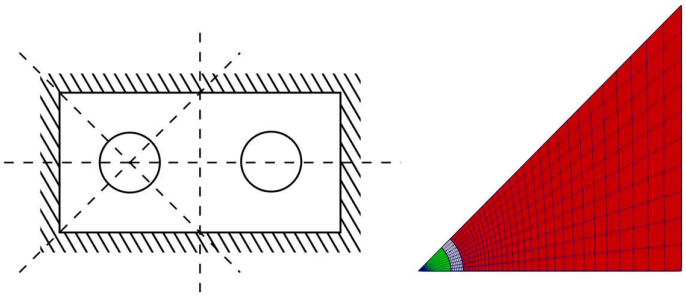

Fig. 5: CFD mesh cut of the simplified storage module geometry. Green: fluid; Gray: steel pipe; Red: concrete.

$$\mathrm{h} = 0.021\frac{d}{k}Re^{0.8}Pr^{0.43}\left(\frac{Pr}{Pr_s}\right)^{0.25} \text{ if } Re > 10^4$$

$$\mathrm{h} = \frac{d}{k}K_0(Re)Pr^{0.43}\left(\frac{Pr}{Pr_s}\right)^{0.25} \text{ if } 2000 < Re < 10^4 \qquad \text{(eq. 4)}$$

$$\mathrm{h} = 0.17\frac{d}{k}Re^{0.33}Pr^{0.43}\left(\frac{Pr}{Pr_s}\right)^{0.25} \text{ if } Re < 2000$$

The final design is selected considering heat transfer performance, hydraulic conditions, and assembly cost of the exchanger. Heat transfer is evaluated using a computational fluid dynamics multi-region OpenFOAM [Weller et al., 1998] solver, hydraulic resistance according to the Handbook of Hydraulic Resistance [Idel′chik, 1996], and assembly cost based on local pricing information.

External CSU insulation is calculated for the selected alternative. Thermal insulation is selected to withhold CSU minimal temperature above the operating cold temperature for 7 days, starting from a fully charged condition, considering winter weather temperatures. The charge loss can be calculated using Equation 5.

$$T(t) = T_\infty + (T_i - T_\infty)e^{-\frac{UA}{mC_p}t} \qquad \text{(eq. 5)}$$

Where UA is the heat transfer coefficient from concrete temperature to exterior air, mC_p is the CSU and thermal inertia. Note that, the thermal inertia of the insulation is not considered, and the cooling rate is considered slow enough for concrete temperature to be considered homogeneous. The insulation thickness can be determined by the determination of the *UA* coefficient.

4. Results and ongoing developments

4.1. Concrete mixture formulation and evaluation

The final concrete formulation (Table 1) corresponds to a self-compacting concrete per cubic meter. A superplasticizer additive was used to achieve maximum mix compaction and to simplify placement, as vibration was not required after filling.

Table 1. Concrete mix for 1 m³

Item	Portland cement CPN 40	Fine sand	Coarse sand	Gravel 5-15	Superplasticizer	Water
Quantity (kg)	467.3	164.5	698.1	908.4	3.8	186.9

Thermal conductivity test results for samples with fiber concentrations of 0, 50, 150 and 250 kg/m3 are presented in Figure 6, where average values and 95% confidence are plotted. The average measured thermal conductivity of the entire sample set is 2.23 W/mK. The samples without metallic fiber content exhibit the highest average thermal conductivity k_0=2.65 W/mK. The observed reduction in thermal conductivity with the addition of metallic fibers may be associated with a rise in sample porosity.

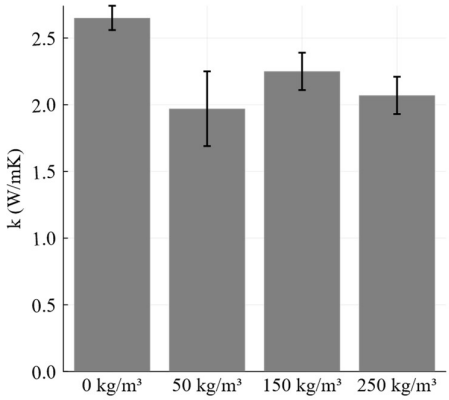

Figure 6: Thermal conductivity measurements at room temperature for different metallic fiber concentration samples.

The implemented testing method presented difficulties when measuring the thermal conductivity of the sample group. Accurate measurements require good thermal contact between the needle probe and the hole wall, which depends on the correct application of thermal paste. However, due to geometric imperfections in the 6 mm diameter measuring hole and considering sample holes are closed on one side of the specimen, no reliable way to ensure complete air evacuation during needle insertion was found. As a result, repeatability issues were encountered, along with handling difficulties when attempting to perform tests at temperatures significantly different from ambient conditions.

An alternative measurement setup, consisting of a thermal bath, is currently under development. In this configuration, thermal conductivity can be indirectly determined during the cooling or heating process of a concrete sample by applying the transient heat transfer equation in conjunction with temperature measurements at the samples center and surface.

4.2. Concrete storage unit shape and dimensions design

The CSU geometry is selected to promote thermal stratification, minimize heat loss through its external envelope, facilitate construction, and reduce the required installation footprint. A schematic of the prototype CSU is shown in Figure 7. The unit consists of five concrete sections (blocks or separations) with embedded zigzagging pipes. A 50 mm glass wool layer is placed between each block to preserve thermal stratification. This configuration provides a greater effective heat transfer length (five times that of a single concrete block) without requiring excessive extension in any single direction.

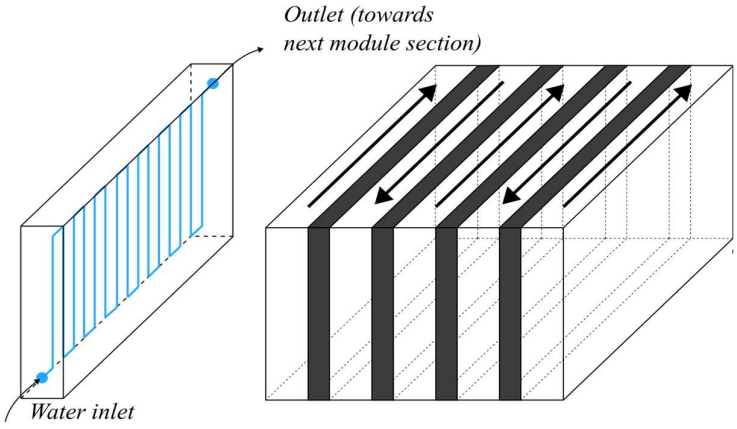

Figure 7: CSU scheme.

Ten initial pipe geometry alternatives were evaluated for a total heat transfer area of 12 m²; however, only three of the proposed CSU configurations exhibited acceptable pressure drops. The main parameters of the suitable alternatives are summarized in Table 2.

Table 2: Suitable alternatives for CSU design.

Alternative	*ND*	*N°*	*L (m)*	$\%\Delta p_{max}$	*h (W/mK)*	*Cost*
1	1/4''	6	46,5	39,9	2410	1.44
2	3/8''	3	74.0	47,1	2560	1.33
3	1/2''	2	89,7	18,5	1790	1.00

Where *ND* represents the nominal diameter of the embedded tubes, *N°* the number of parallel lines in each concrete block, *L* the total pipe length across the five blocks, and $\%\Delta p_{max}$ the percentage of the allowable pressure drop used by the CSU. The coefficient *h* denotes the convective heat transfer coefficient, and *Cost* is expressed relative to the least expensive alternative. The concrete heating rate and stored energy for each configuration are presented in Figure 8. Although alternatives 1 and 2 exhibit slightly better thermal performance, the improvement over alternative 3 is not sufficient to justify the associated cost increase. Furthermore, due to its lower cost and reduced pressure drop, alternative 3 offers a suitable base design from which new configurations could be developed by extending pipe length, while still maintaining lower cost and pressure drop compared to alternatives 1 and 2.

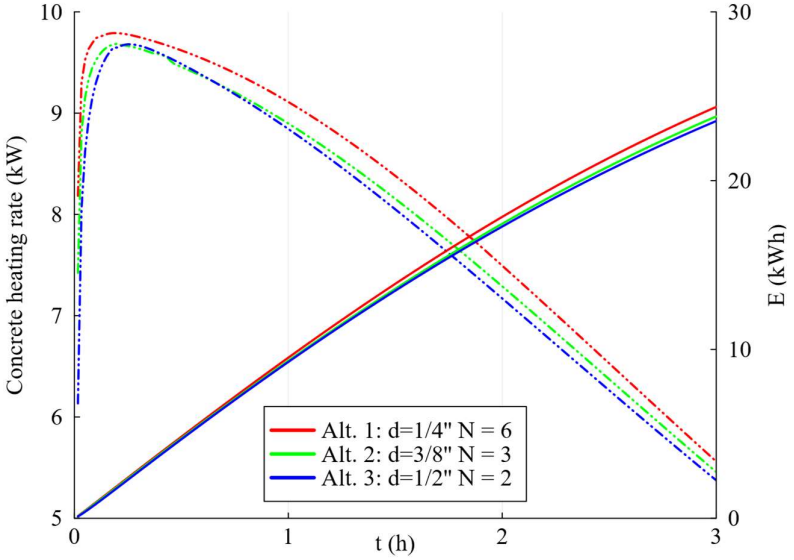

Figure 8: Thermal performance comparison of suitable CSU alternatives via concrete heating rate and non-dimensional stored energy E*.

Given that the budget allows for a more expensive CSU, a larger version of alternative 3 was selected, increasing the pipe length by a factor of 1.2. Although the pipe length is extended, the total concrete mass can be maintained by "stretching" the concrete region and placing the tubes closer together. A comparison of heat transfer performance between the enlarged pipes and concrete configuration (referred to as *larger*) and the version with only enlarged pipes (referred to as *extruded*) is shown in Figure 9. The State of Charge (SOC) is calculated using Equation 6, and the heat rate corresponds to the difference in enthalpy flux between the inlet and outlet.

$$SOC = \frac{1}{I_{CSU}(T_h - T_c)} \int_{\Omega} \rho C_p (T - T_c) dV \qquad \text{(eq. 6)}$$

Where $I_{CSU} = \sum mC_i$, represents the thermal inertia of the CSU, with the subscript i referring to each constituent material (pipe, water, and concrete), T_h and T_c are the hot and cold reference temperatures, and Ω is the control volume encompassing the entire CSU.

Both the *larger* and *extruded* configurations exhibit improved thermal performance compared to the base alternative (No. 3). Stored energy and charging rates increase in both cases, while thermal stratification is more pronounced in the *extruded* alternative, as shown in the Heat Rate versus SOC plot. For a given SOC, the *extruded* configuration achieves higher charging rates than the other CSU arrangements. The predicted behavior indicates that this configuration generates larger concrete regions where the temperature potential remains higher.

Given that the relative increase in construction cost for the *extruded* alternative is smaller than the enlargement factor of 1.2 (within the available budget) and that thermal performance improves significantly, the *extruded* version of alternative 3 was selected as the CSU geometry. Thermal stratification is also observed in the temperature distribution, which is presented at different stages of the charging process in Figure 10. Here, θ^* is the non-dimensional temperature, calculated from Equation 7, and x^* is the non-dimensional length x/L, with T_c and T_h denoting the cold and hot reference temperatures.

$$\theta^* = \frac{T - T_c}{T_h - T_c} \qquad \text{(eq. 7)}$$

At the beginning of the charging stage, significant temperature differences exist both axially and transversally. However, as charging progresses, the temperature gradient in the transversal direction decreases. For most of the charging period, transversal temperature differences remain approximately constant, consistent with the initial design hypothesis.

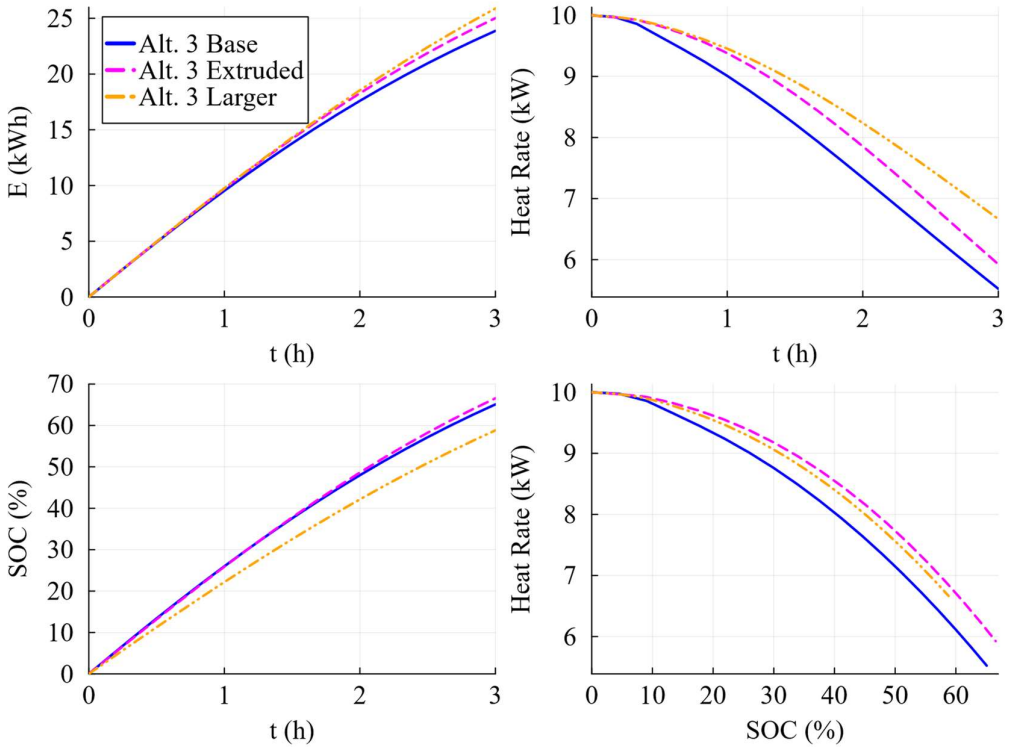

Figure 9: Comparison of thermal performance for alternative 3 variations: base, extruded and larger.

There are two key aspects to consider when interpreting these results. First, the predictions have not yet been validated experimentally, and therefore the actual prototype behavior may differ from the simulated outcomes. Nevertheless, the results are consistent with heat transfer theory, as the variations expected to improve thermal stratification are reflected in the simulations. Further testing with the constructed prototype will allow evaluation of the proposed heat transfer model and provide insights for its refinement in future analyses of CSU enhancements.

Second, the simulations assume a constant flow rate and input temperature, whereas in real operation, the flow rate will vary to maintain a relatively stable input temperature. Consequently, the actual behavior of the CSU's heat transfer fluid (particularly the flowrate) may deviate from the simulated scenarios. Further evaluation of

the CSU performance under varying operating conditions is therefore needed to improve predictions of energy storage and CSU charging/discharging rates.

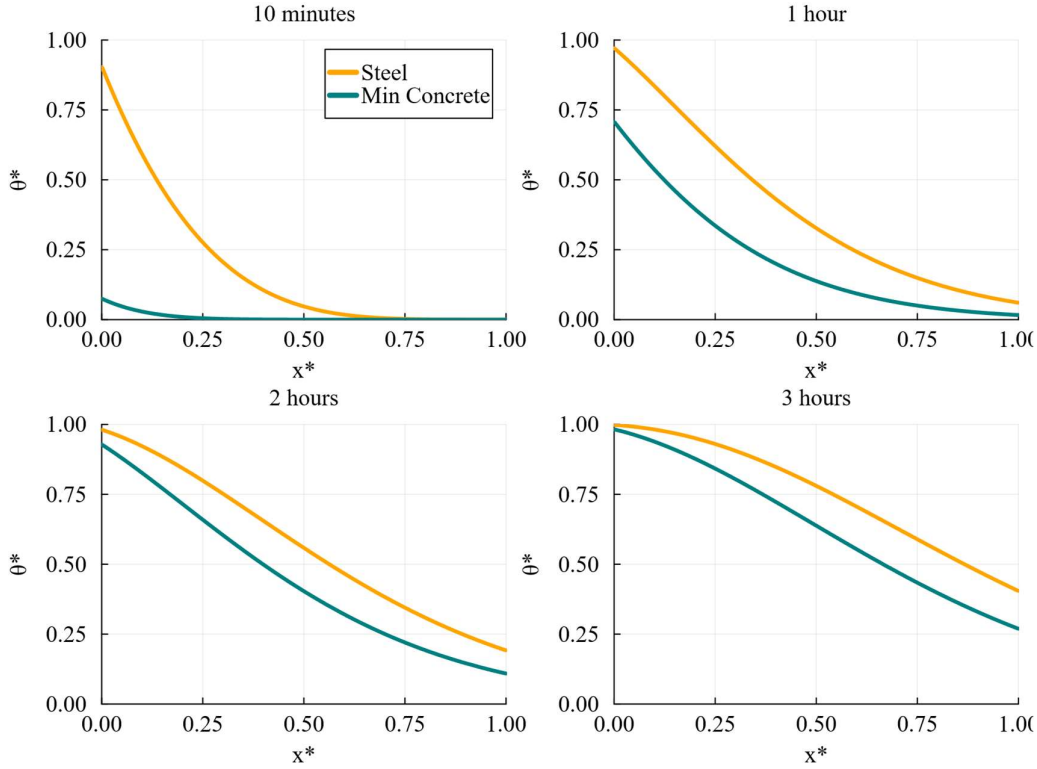

Figure 10. Non-dimensional temperature difference distribution during the charging period: t=10min, 1h, 2h and 3h

5. Conclusions

The design process of a CSU with a focus on low fabrication costs and thermal performance was carried out, including the evaluation and design of both the concrete mixture and the CSU geometry.

The concrete mixture formulation was guided by recommendations from previous literature and included an analysis of the impact of metallic fiber additions. Thermal conductivity of concrete samples with varying metallic fiber content was measured at room temperature using a TEMPOS needle probe. The average thermal conductivity of the mixture without metallic fibers was k=2.65 W/mK. For the tested samples, the inclusion of metallic fibers appeared to reduce thermal conductivity, possibly due to increased porosity, although further testing is required to draw definitive conclusions. The testing process proved challenging, with reproducibility issues observed, indicating that the implemented method is not fully adequate for accurate thermal conductivity determination; therefore, an alternative measurement approach is being considered.

The CSU shape and dimensions were evaluated considering cost, hydraulic performance, and thermal behavior. The selected geometry consists of a concrete matrix divided into five blocks, each containing two embedded zigzagging pipes. Blocks are separated by a 50 mm thick glass wool layer to preserve thermal stratification. Dimension selection involved comparing alternatives with the same total heat transfer area, evaluating thermal performance and construction cost while ensuring suitable pressure drops. The final design uses two ND 1/2'' SCH40 pipes, each 107.6 m long, for a total heat transfer area of 14.4 m². Simulations suggest that this alternative achieves a favorable degree of thermal stratification while keeping prototype costs within budget.

Although the simulation results are consistent with theoretical expectations, experimental validation is still pending, and prototype behavior may differ from predictions. Model calibration and evaluation will be performed once the CSU prototype is constructed. Furthermore, future analysis should consider varying

operating conditions, including flow rate variations and different initial charging states, ideally in combination with a thermal model of the entire installation.

6. Acknowledgments

The authors gratefully acknowledge the National Agency of Research and Innovation (ANII) of Uruguay for its financial support through project ANII_ART_X_2023_1_179571 “Calor y acumulación solar para la industria”.

7. Declaration of generative AI and AI-assisted technologies in the writing process

During the preparation of this work the authors used ChatGPT in order to improve the readability and language of the manuscript. After using this tool/service, the authors reviewed and edited the content as needed and take full responsibility for the content of the published article.

8. References

Asadi, I., Shafigh, P., Abu Hassan, Z. F. B., & Mahyuddin, N. B. (2018). Thermal conductivity of concrete A review. Journal of Building Engineering, 20, 81–93. https://doi.org/10.1016/j.jobe.2018.07.002.

Boquera, L., Castro, J.R., Pisello, A.L., Cabeza, L.F., 2021. Research progress and trends on the use of concrete as thermal energy storage material through bibliometric analysis, Journal of Energy Storage. 38.

Cook, D. J., & Uher, C. (1974). THE THERMAL CONDUCTIVITY OF FIBRE-REINFORCED CONCRETE. Cement and Concrete Research, 4(4), 497–509.

Dellicompagni, P., Hongn, M., Saravia, L., Altamirano, M., Placeo, C., Gea, M., Hoyos, D., Bárcena, H., Suligoy, H., Fernández, C., & Caso, R., 2021. Concentrador solar termico fresnel lineal de San Carlos, Salta. Primeros ensayos de operación y funcionamiento (172m2). *Avances En Energías Renovables Y Medio Ambiente - AVERMA*, *20*, 1–12.

Haller M.Y., Cruickshank C.A., Streicher W., Harrison S.J., Andersen E., Furbo S., 2009. Methods to determine stratification efficiency of thermal energy storage processes – Review and theoretical comparison, Solar Energy. 83. 1847-1860.

Idel’chik, I.E. (1996) Handbook of Hydraulic Resistance. 3rd Edition, Begell House Inc., New York.

Kodur, V. K. R., and M. A. Sultan. "Effect of Temperature on Thermal Properties of High-Strength Concrete." *Journal of Materials in Civil Engineering*, vol. 15, no. 2, 2003, pp. 101–107. *ASCE Library*, doi:10.1061/(ASCE)0899-1561(2003)15:2(101).

Laing, D., Lehmann, D., Bahl, C., 2008. Concrete Storage for Solar Thermal PowerPlants and Industrial Process Heat. Proceedings: Third International Renewable EnergyStorage Conference, November, 2008.

Laing, D., Steinmann, W.D., Tamme, R., Worner, A., Zunft, S., 2012. Advances in thermal energy storage development at the German Aerospace Center (DLR). Energy Storage Science and Technology 1.

Liang, S., Song, G., Du, H., Li, X., Liu, J., & Wei, Y. (2023). Mesoscale FE analysis of thermal conductivity of steel fiber-reinforced cementitious materials considering fiber-matrix interface and pore effects. Cement and Concrete Composites, 142, 105194. https://doi.org/10.1016/j.cemconcomp.2023.105194.

Mikheyev, M. (1968). Fundamentals of heat transfer. Moscow: Mir Publishers.

Sarbu, I., Sebarchievici, C. (2018). A Comprehensive Review of Thermal Energy Storage. *Sustainability*. *10*.

Tempos (2024). Tempos Manual. 18215-10 5.2024.

Weller H. G. , Tabor G., Jasak H., Fureby C., A tensorial approach to computational continuum mechanics using object-oriented techniques, COMPUTERS IN PHYSICS, VOL. 12, NO. 6, NOV/DEC 1998.

Zhang, Y., Lei, Q., Zhao, W., Yang, Y., Wang, Y., Yan, Z., Zhu, H., & Ju, J. W. (2023). An improved micromechanical model for the thermal conductivity of multi-scale fiber reinforced ultra-high performance concrete under high temperatures. Materials & Design, 236, 112503. https://doi.org/10.1016/j.matdes.2023.11250 3.